Additive Manufacturing 97 (2025) 104612

Contents lists available at ScienceDirect

Additive Manufacturing

journal homepage: www.elsevier.com/locate/addma

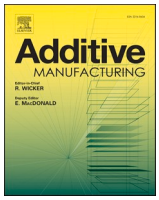

Vacuum-assisted extrusion to reduce internal porosity in large-format additive manufacturing☆

Frye Mattingly [a], Vipin Kumar [b], Komal Chawla [b], Wim Bras [c], Vlastimil Kunc [b], Chad Duty [a,b,*]

[a] Department of Mechanical, Aerospace, and Biomedical Engineering, University of Tennessee, Knoxville, TN 37996, USA
[b] Manufacturing Science Division, Oak Ridge National Laboratory, Knoxville, TN 37932, USA
[c] Chemical Science Division, Oak Ridge National Laboratory, Oak Ridge, TN 37831, USA

ARTICLE INFO

Keywords:
Porosity
Microstructure
Large format
Fiber reinforced
3D printing

ABSTRACT

Large-scale 3D printing of polymer composite structures has gained popularity and seen extensive use over the last decade. Much of the research related to improving the mechanical properties of 3D-printed parts has focused on exploring new materials and optimizing print parameters to improve geometric control and minimize voids between printed beads. However, porosity at the microstructural level (within the printed bead) has been much less studied although it is almost universally observed at levels of 4 %-10 % when using fiber reinforced materials. This study introduces a vacuum-assist approach that minimizes internal porosity by removing ambient air from the interstitial space between pellets in the hopper and acts as a negative pressure vent for gases that evolve during the initial stages of single-screw extrusion. Vacuum-assisted extrusion was able to reduce porosity below 2 % across a wide range of processing parameters, moisture content, fiber reinforcements, and printing platforms. Specifically, when printing on a large-format extruder (Strangpresse Model-30), the vacuum-assisted extrusion reduced internal porosity by 35–75 % compared to conventional non-vacuum extrusion, and only pores with length scale > 2 microns are affected. The success of this approach prompted the design of a patent-pending continuous vacuum hopper relevant for large-scale 3D printing on commercial systems.

1. Introduction

Over the past decade, large format additive manufacturing (LFAM) has enabled the direct printing of large-scale structures on the order of multiple meters as well as tooling for aerospace and automotive applications [1]. One of the earliest manifestations of this technology was the Big Area Additive Manufacturing (BAAM) system developed by Oak Ridge National Laboratory in collaboration with Cincinnati Inc. [2]. The BAAM system introduces pelletized feedstock materials into a single-screw extruder to deposit material through an orifice with a 5.08–10.16 mm diameter. The BAAM system is capable of depositing over 45 Kgs of material per hour in a build volume of 6.1 m (Length) x 2.44 m (Width) x 1.83 m (tall) and has been used to print large structures such as automobiles, submersible vehicles, and houses. Advancing the LFAM from a gantry to a robotic motion platform, ORNL has also developed a highly automated manufacturing process for thermoplastic composite that combines the benefits of Additive Manufacturing and Compression Molding (AM-CM) to produce high-performance functional composite structures at automotive production rates. The AM-CM process consists of a six-axis robot (Kuka Robotics) with a payload of 300 kg; a system for feeding material (Dri-Air Industries, Inc.). A 68 kg/h extruder (Strangpresse Model-30) with a material-feeding mechanism is mounted atop the robot and can be picked and dropped very quickly, allowing the swift transition between various printing materials [3,4].

Large-scale AM structures tend to distort during printing due to uneven cooling and sequential solidification of the printed layers. As a result, most LFAM structures utilize a fiber-reinforced feedstock material, such as 20 wt% carbon fiber reinforced acrylonitrile butadiene

* Corresponding author at: Department of Mechanical, Aerospace, and Biomedical Engineering, University of Tennessee, Knoxville, TN 37996, USA.
E-mail address: cduty@utk.edu (C. Duty).

https://doi.org/10.1016/j.addma.2024.104612
Received 5 January 2024; Received in revised form 14 December 2024; Accepted 15 December 2024
Available online 17 December 2024

styrene (20 %CF-ABS), to increase stiffness and minimize distortion [5, 6]. Most fiber-reinforced materials are used in a pelletized format, with a pellet length of around 3 mm and an average fiber length of less than 500 microns. During the LFAM extrusion process, the fibers preferentially align with the primary axis of the deposited bead (x-axis), especially along the bead's outer surface [7]. Along with the layered structure inherent to a 3D printed part, the preferential alignment of fibers leads to significant mechanical anisotropy, where the through-thickness strength (z-axis) can be a small fraction (<10 %) of the strength in the printed bead direction (x-axis) [8].

The majority of studies related to the mechanical performance of LFAM structures have investigated the effects of printed parameters on the deposited meso-structure, including such variables as the bead geometry [9], inter-bead porosity [10], and inter-layer bond quality [11, 12]. However, the problem of intra-bead porosity has received much less attention, but it is also an essential factor in the performance parameters of printed objects. The current study focuses on the ***internal*** microstructure of a printed bead, specifically related to the presence of ***intra-bead porosity*** that has been almost universally observed in LFAM structures when depositing fiber-reinforced materials. Fig. 1 shows a typical cross-section of a part printed with 20 %CF-ABS with significant internal porosity. Note the high concentration of circular pores (dark spots) that range from 50 to 100 microns in diameter compared to the smaller light gray reinforcing fibers that are 7 microns in diameter. Earlier work indicated that internal porosity could account for as much as 4–20 % of the volume of the printed bead, depending on print conditions [13,14].

The porosity within a printed bead could originate from several sources during the extrusion of a fiber-reinforced thermoplastic. **(I)** One potential source of porosity is absorbed moisture in the pelletized feedstock material. Several thermoplastic materials used for 3D printing are hydrophilic (e.g., nylon), and can absorb significant amounts of moisture if stored in a humid environment [15]. During deposition at elevated temperatures, the absorbed moisture will evolve as water vapor, likely forming a small bubble that will grow in volume as the pressure is reduced when the extrudate exits the orifice. **(II)** A second source of porosity could be ambient gases surrounding the pellets while stored in the feed hopper. As the loosely packed pellets are gravity-fed into the extrusion screw, ambient gases may be trapped in the interstitial spaces and become integrated into the molten flow of plastic as gas bubbles. **(III)** A third source of porosity is the evolution of dissolved gases in the polymer material, which may have been introduced to the material in a prior processing step (e.g., pelletization) and are then evolve as gas bubbles as pressure is reduced in the molten polymer during the extrusion process. **(IV)** A fourth source of porosity could be the gaseous byproducts of thermal degradation of the polymer matrix during the extrusion process. The temperature profile of a well-designed extruder should not exceed the degradation temperature of the polymer, but it is possible that the process has a local temperature variation or is poorly controlled. **(V)** A final source of porosity could be cavitation as a long reinforcing fiber accelerates through the extrusion orifice, creating a vacuum void in the trailing polymer matrix. If this were the case, one would expect to see a strong correlation between porosity and shear rate in the extrusion orifice and to find a high percentage of voids localized around the ends of fibers.

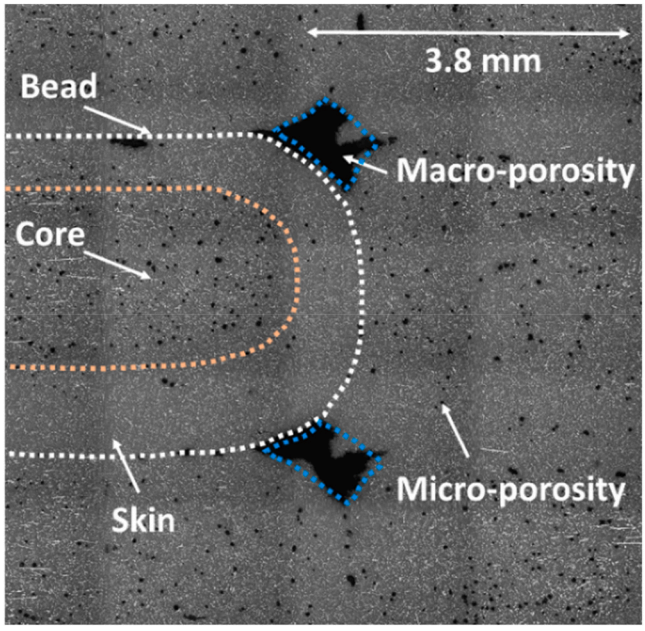

Fig. 1. Optical micrographs of BAAM sample; high porosity is present between the interphase of the printed beads (in a diamond shape); it is the macro-porosity. The bead's porosity shows a skin-core-skin effect in which significantly less porosity in the skin area and higher porosity in the core zone is observed.

A few approaches have been quite effective at minimizing the internal porosity of fiber-reinforced materials in more conventional manufacturing techniques, such as injection molding and conventional extrusion. An obvious approach to minimizing moisture **(I)** in a pelletized feedstock is to dry the material for several hours at elevated temperatures just before deposition (typical for CF-ABS: 4 hours at 85° C). For LFAM applications that require a small and portable feedstock hopper, a separate drying tower is typically located beside the printer, and small volumes of pellets are pneumatically transported to the on-board hopper as needed. Long-term storage of pelletized feedstock should also be carefully controlled to avoid exposure to high humidity conditions before drying. Another approach used in traditional extrusion screw systems to avoid trapped gases **(II)** and evolution of gases during processing **(III, IV)** is the use of a vented screw. A vented screw design has a few flights following the compression section that momentarily reduce the system pressure inside the barrel and have a port to the ambient air that allows trapped gases to escape [16]. Vented screws are typically longer and weigh more than non-vented screws, and the extrusion systems are more complex and expensive – all of which are disadvantageous when considering a portable extrusion system for LFAM, especially a robotic LFAM system, where payload and space is limited. Furthermore, traditional injection molding systems also have the advantage of injecting material into a mold at high pressure, discouraging pore nucleation and growth until the material cools and solidifies. This is not an option for LFAM extrusion systems that deposit into ambient conditions.

This study aimed to minimize the internal porosity of printed fiber-reinforced beads relevant to LFAM applications. It was desired to avoid the use of a vented screw design to minimize the weight, complexity, and cost of the LFAM extrusion system. It was hypothesized that applying a partial vacuum to the feed hopper would reduce air entrapment and significantly reduce porosity (preceded, of course, by thoroughly drying the feedstock material). The effect of fiber content in the polymer on the porosity was also studied in this work since similar amounts of porosity had not been observed in neat (unreinforced) materials. Therefore, it was further hypothesized that the surface of reinforcing fibers served as nucleation sites for pores, so the amount of porosity would increase with fiber wt% content.

2. Experimental procedure

A series of experiments were designed to evaluate the effectiveness of applying a partial vacuum to the pellet feed hopper to reduce the porosity in the extruded beads. A small batch "vacuum hopper" approach was developed for extruding material using a benchtop extrusion platform from Randcastle as well as a larger Strangpresse extruder (Model-30) used on the AM-CM system. The ability of the vacuum hopper to reduce porosity was evaluated for feedstock materials under different

drying conditions, as a function of screw speed (shear rate), and for varying amounts of fiber content.

2.1. Extrusion platforms

An approach for extruding small batches of material under a partial vacuum was developed on two separate platforms: a benchtop single-screw extruder from Randcastle (Fig. 2a) and a Strangpresse single-screw extruder (Fig. 2b) used on the AM-CM system.

The Randcastle benchtop system (model RCP-500, serial J2697) is a vertically-oriented single screw extruder with a roughly 3.5 liter pellet hopper sitting directly above a 12.7 mm diameter screw. The screw section is 61 cm long and has four thermal zones that were set to 180 °C (feed section), 220 °C (mixing section), 240 °C (metering section), and 240 °C (exit manifold). The manifold at the end of the screw turns the material 90 degrees to exit horizontally through a 6.35 mm diameter nozzle (Fig. 3a). The screw rotational speed was varied from 40 to 110 RPM in increments of 10 RPM. Most samples within this research were collected at a constant 100 RPM unless otherwise specified. In order to apply a vacuum to the pellet hopper, an aluminum lid with a vacuum port and a pressure gauge was placed over the hopper (Fig. 3b). After loading the pellets (60–80 g per sample set) and establishing consistent extrusion under ambient conditions, the vacuum lid was put in place, the vacuum pump (ULVAC model GLD-135C, 135–162 L/min) was turned on, and a rough vacuum of −25 inHg gauge pressure (-646 Torr) was achieved in the hopper within 5–10 seconds of the pump being activated under constant extrusion. A visual inspection of the bead shape, quality, and color would determine roughly when a steady state had been reached. As an example of visual differences, compare the beads in Figs. 3a and 3c. In Fig. 3a, the bead surface shows signs of shark-skinning and has undergone die swell as it exited the nozzle. By contrast, the bead in Fig. 3c is smooth and of even diameter. However, shark-skinning behavior reappeared during experiments with the Strangpresse extruder (Model-30), suggesting the need for fine-tuning of vacuum pressure to achieve consistent bead quality.

The larger-scale Strangpresse single-screw extruder (Model-30) is used on the AM-CM printing system. The extruder used in this study was a vertically-oriented single-screw extruder with a 30 mm diameter screw that was 914.4 mm long. The motor is a max 3000 RPM motor with a 1:5 gearbox making the screw speed 1/5 of the motor speed. The RPM mentioned for the Strangpresse extruder in this study is the motor RPM. A 2.1 liter prismatic pellet hopper (Fig. 4) was designed specifically for these experiments that was positioned above and slightly offset from the screw axis. Pellets were gravity-fed through a port in the side of the barrel using a 25.4 mm in diameter angled tube. The extruder used four temperature control zones along the length of the screw set to 180 °C (feed section), 220 °C (mixing section), 240 °C (metering section), and 240 °C (nozzle). At the end of the screw, the material exits vertically through a 10.16 mm diameter nozzle. The motor rotational speed was tested at 400 RPM and 800 RPM. Similar to the Randcastle system, a lid was designed for the Strangpresse hopper, including a vacuum port and pressure gauge. After consistent flow had been established, the vacuum lid was placed on top of the hopper, a vacuum pump (CPS model VP4D, 96 L/min) was turned on, and a rough vacuum of −10 to −15 inHg (-254 to −381 Torr) was achieved in the hopper within 2–3 minutes under constant extrusion. Extruded samples were vertically suspended in around 500–600 mm sections before being trimmed at the nozzle exit and transitioned to a horizontal tray for cooling.

2.2. Material and drying procedures

Three material sources were used in these experiments to evaluate the effect on porosity due to increasing the amount of fiber reinforcement and changing the type of reinforcing fiber. All materials were procured commercially in pellet form. Acrylonitrile butadiene styrene (ABS) is one of the most widely used polymer systems for large-scale additive manufacturing. Since the final aim for the vacuum-assisted extrusion is to be implemented on the LFAM system, ABS was selected for this study. ABS was supplied by TechmerPM (product # 5 MFI High Impact ABS). The two reinforced materials were 20 wt% carbon fiber ABS (product # ELECTRAFIL J-1200/CF/20 3DP) and 40 wt% glass fiber ABS (product # HIFILL ABS 1601 3DP), also supplied by

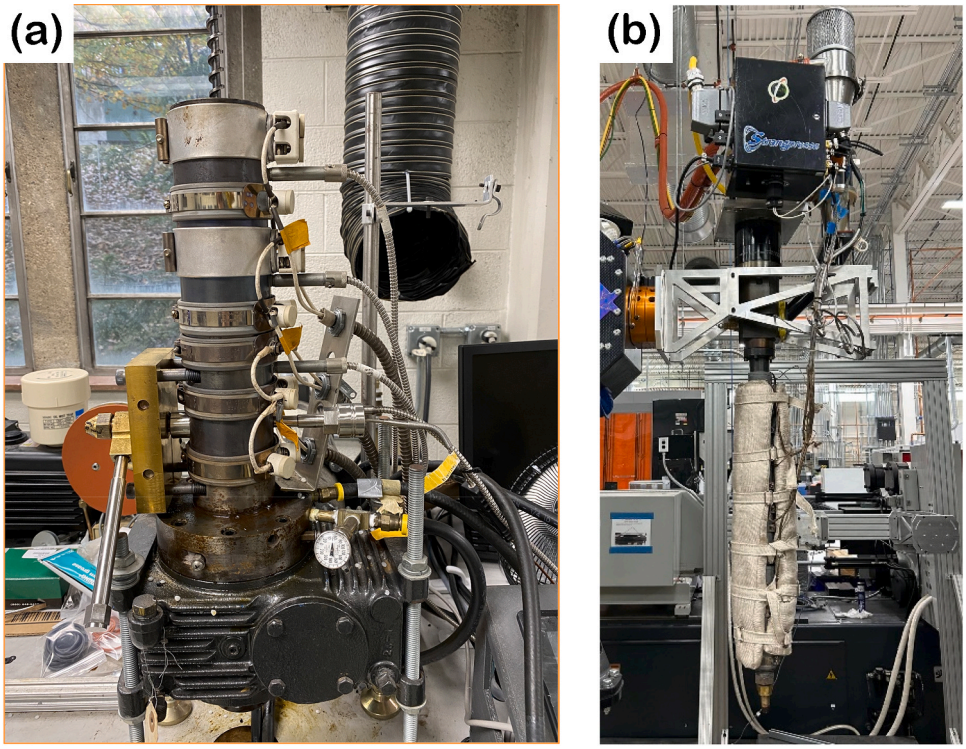

Fig. 2. (a) Benchtop Randcastle extruder (b) The large-scale Strangpresse extruder (Model-30).

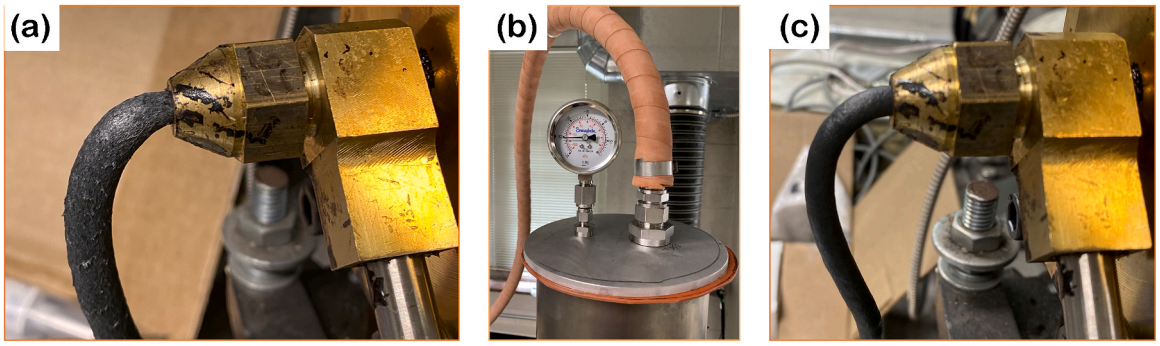

Fig. 3. (a) Extrusion of 20 %CF ABS from the Benchtop Randcastle showing die swell and sharkskinning (b) The Vacuum gauge of the added sealed lid showing an achieved vacuum of −25 inHg (-646 Torr) (c) Extrusion of 20 %CF ABS while vacuum was applied to the system showing no visible die swell and a smooth bead surface.

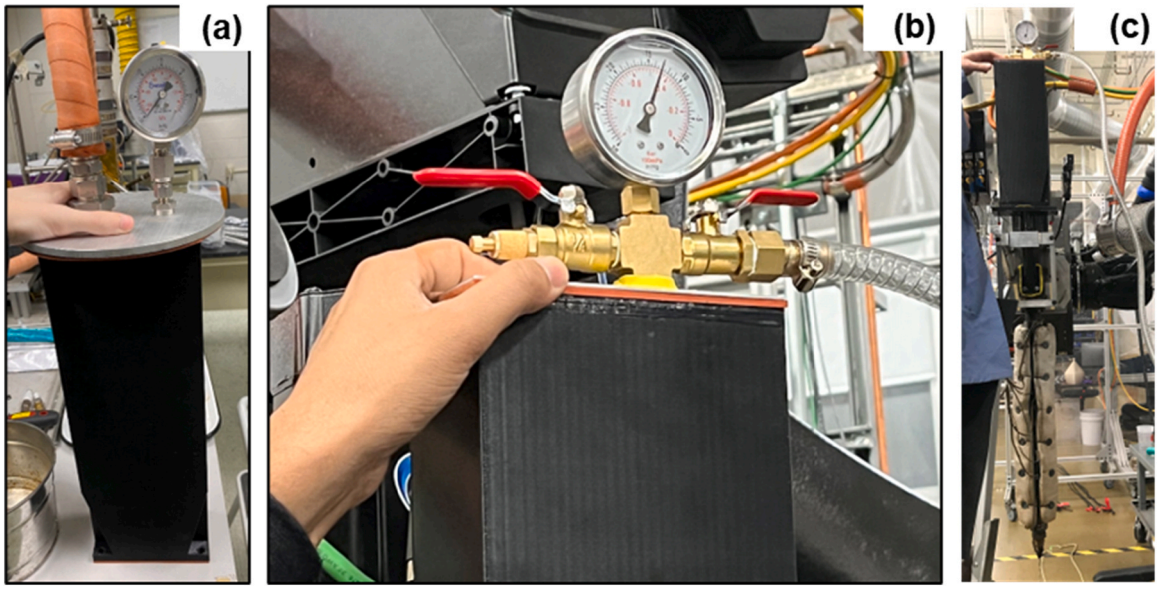

Fig. 4. (a) The prismatic hopper's ability to hold vacuum was validated before installation on the extruder (b) The vacuum gauge shows that a vacuum of about −13 inHg (-330 Torr) was achieved on the Strangpresse system (c) The hopper was mounted to the system slightly above and offset from the screw axis and the junctions were sealed with putty.

TechmerPM. In order to vary the reinforcement content, the reinforced materials were down-blended in pelletized form with neat ABS. Before extrusion, the materials were dried at 80 °C for at least 8 hours. In order to test the effect of moisture uptake on porosity, some samples were left in a container (covered and uncovered) on the benchtop at ambient conditions (22 °C, 50–65 % relative humidity) for up to 6 hours.

2.3. Characterization techniques

The porosity of extruded samples was evaluated using a volume-based Archimedes technique [14]. Samples were typically cut into 2–3 cm long segments and measured individually. Each measurement recorded represents the average and standard deviation of at least 5–7 separate measurements of adjacent segments from a single extruded bead. Plotting the data from these samples sequentially confirmed that the measured samples had achieved a steady state (Fig. 5). Every point on the plot is a 2.54 mm slice of material, with the X-axis showing the relative positions of each bead throughout the entire extrusion. The blue region shows the transition from purge material to non-vacuum steady state, so the final cluster of points from ~ 100 cm to 125 cm would be averaged to form a single datapoint for the non-vacuum condition (9.1 % porosity with a 0.41 % standard deviation). The orange region

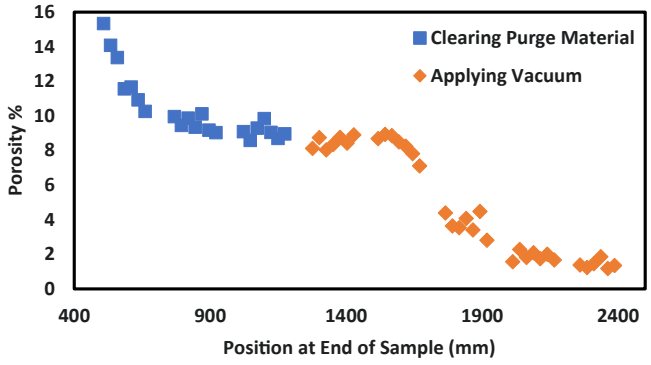

Fig. 5. Porosity due to moisture absorption after 2 hours in a covered container. The blue region indicates porosity as the purge material (non-vacuum) is cleared. The orange region indicates porosity after the vacuum was applied.

shows the transition from non-vacuum to vacuum and then to the final steady state. Again, the final cluster of samples would be averaged into a single data point for the vacuum condition (1.3 % porosity with a

0.28 % standard deviation). The process for determining the porosity of the material involves measuring the dry weight of the sample as well as the weight once submerged under water. The weight change then determined the density of the sample due to buoyancy, and the porosity was determined by comparing the measured density against a "fully dense" control sample made by injection molding. For samples where the tested fiber loading had been down-blended to a nonstandard value, the control density was calculated through linear interpolation between the densities of molded bars at typical maximum fiber loading and another made of neat ABS. The scale used for these measurements was a Mettler Toledo Excellence Level and an XS series Analytical Balance.

Soft X-ray Computed Tomography (XCT) was employed to validate the porosity results and was performed at the Advanced Light Source (Berkeley) on beamline 8.3.2, using an X-ray photon energy of 10 keV, which is optimal for the imaging and XCT of carbon-based materials [17]. The soft XCT method is more accurate compared to the Archimedes technique as it helps to capture the 3-dimensional morphology of the pores; however, it is an expensive and time-consuming process; therefore, only a limited number of samples were analyzed using XCT. The ImageJ software, an open-source tool, was applied for the processing and analysis of the XCT images. The XCT images, called slices, were initially imported into the ImageJ software. For each process (vacuum and non-vacuum), 186 XCT slices were imported and transformed into 8-bit greyscale images. These binary images were well-suited for thresholding and remained manageable for software processing. The XCT images were usually accompanied by a scale bar, facilitating the conversion of pixel measurements into tangible units. This conversion aided in quantifying pixel dimensions within the pores using the desired units. Subsequently, the images were cropped to achieve an optimal sample view. The application of an automatic color balance led to a clear differentiation between the pores and the matrix, achieved by darkening the interior pore area. A Kalman stack filter was implemented to enhance image quality to eliminate high-grain noise from the stacks, resulting in a smoother portrayal of pore transitions across slices. The threshold function was then applied and carefully adjusted to identify a maximum number of pore pixels while minimizing the inclusion of matrix pixels. Following this, the "Close" function within the process tab was executed, involving dilation followed by erosion operations to refine the image, achieving smoothing effects and filling small voids. A stack of 186 images was used after removing any outlier from the stack to compute porosity from the XCT images.

The porosity of extruded samples was also investigated using small-angle X-ray scattering (SAXS). Since smaller porosity (nm-scale) cannot be investigated using optical microscopy or even most tomography approaches, SAXS was utilized to evaluate the effect of the vacuum hopper on pores below 300 nm in diameter (the upper limit of SAXS sensitivity); if there are any. The presence of smaller diameter pores in the printed sample was considered to result from either thermal degradation or outgassing of dissolved gases (sources **III** and **IV**) since they likely occurred near the end of the extrusion process where the temperature was high, and the pressure change was most significant. Pores that had formed earlier in the extrusion process due to moisture (source **I**) or entrapped air (source **II**) would likely coalesce and grow into larger pores during the printing process. Therefore, it was anticipated that the number of smaller pores would be unaffected by the vacuum hopper.

Samples for SAXS were sectioned from extruded beads using the Strangpresse platform at a motor rotational speed of 800 RPM. Samples were cut to a thickness of 2 mm, creating a round disk when cut in the transverse direction or a rectangular plaque when cut parallel to the extrusion direction. SAXS data were obtained using A Xeuss 3 SAXS/WAXS set-up (Xenocs, Holyoke, USA) using an Excillum metal jet generator and a Dectris 4 M Eiger detector.

2.4. Experimental results & discussion

The ability of the vacuum hopper to reduce porosity on the benchtop (Randcastle) extrusion system was measured at various screw speeds, at different levels of moisture absorption, and across a wide range of reinforcement content. A similar vacuum hopper system was evaluated on a large-scale extruder (Strangpresse) to demonstrate the effectiveness of the approach on an LFAM-relevant platform. Finally, the baseline level of smaller porosity, likely unaffected by the vacuum hopper approach, was established using SAXS.

2.5. Effect of vacuum hopper at various screw speeds

Fig. 6 compares the porosity of 20 %CF-ABS samples extruded using the Randcastle benchtop system, in either conventional or vacuum hopper mode, as a function of screw rotational speed. The use of the vacuum hopper was highly effective at reducing the porosity of extruded samples across all screw speeds. The average porosity of samples extruded using the conventional approach (hopper open to ambient air) was ~4 %, whereas the average porosity of samples extruded using the vacuum hopper was ~1.3 % (over a 66 % reduction). There was no apparent relationship between porosity and screw speed, neither using the conventional hopper nor the vacuum hopper approach. There was a considerable variation in observed porosity using the conventional approach (2.6 % – 6.0 %) compared to a relatively small variation in porosity (1.0–1.8 %) when using the vacuum hopper. These tests were repeated twice. Each data point represents five measured samples at each condition on a given day with a single standard deviation shown with error bars. There was a high variance across data sets for the conventional approach; within individual sample sets, the standard deviation could be as high as ± 0.5 %.

2.6. Effect of vacuum hopper at various moisture levels

For this section, 40 %GF-ABS pellets were removed from the drying oven and left on a benchtop in a container, covered or uncovered, for several hours before printing. Fig. 7 shows the porosity of samples stored in a covered container for up to six hours before printing. Using the conventional hopper approach, the porosity of samples that were immediately transitioned to the printer was 5 % - 10 %. When the pellets were stored in a covered container, the porosity increased to 20 % - 25 % within 3–4 hours. The vacuum hopper approach effectively reduced the porosity to below 5 % for the first 3 hours but steadily increased to ~8 % after 6 hours. However, at each condition measured, the vacuum hopper approach significantly reduced the porosity.

The effects on porosity were significant when the 40 wt%GF -ABS samples were exposed to ambient air (uncovered) prior to extrusion. Fig. 8 shows that samples exposed to ambient conditions for even 1 hour had porosity on the order of 25 % when using a conventional hopper and held constant for exposure times approaching 6 hours. The vacuum

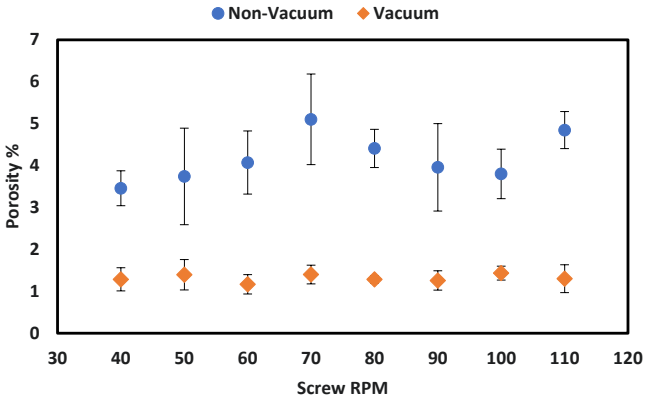

Fig. 6. Porosity of extruded 20 %CF-ABS samples at various screw rotational speeds using the conventional hopper and the vacuum hopper approach.

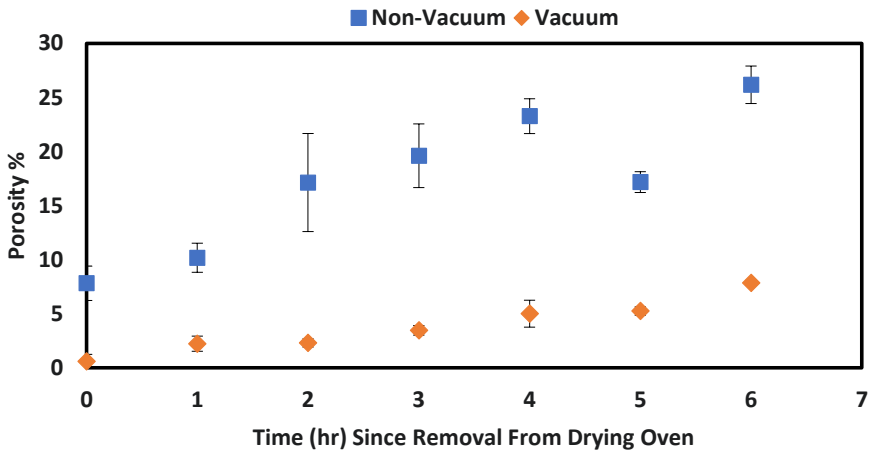

Fig. 7. Porosity of 40 %GF-ABS samples stored in a covered container prior to extrusion with either a conventional hopper or a vacuum hopper.

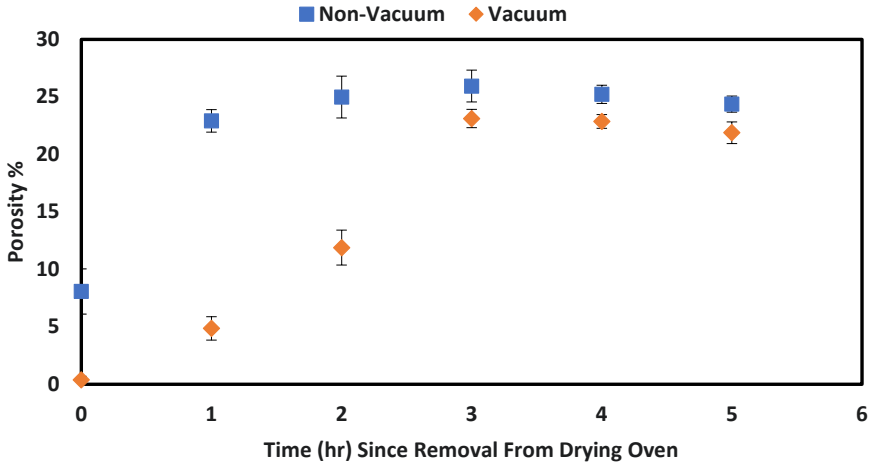

Fig. 8. Porosity of 40 %GF-ABS samples stored in an uncovered container prior to extrusion with either a conventional hopper or a vacuum hopper.

hopper approach was very effective at reducing the porosity of these samples after exposure times of 1–2 hours, but there was relatively little impact of the vacuum hopper system after 3 hours of exposure. It seems that the vacuum hopper was more effective during the shorter exposure times because moisture was primarily concentrated on the surface of the pellets and was likely driven out of the material early in the extrusion process when the negative pressure in the pellet hopper was able to extract it from the system. During more prolonged exposure, moisture likely penetrated deeper into the core of the pellets and did not evolve as a gas until later in the extrusion process when it was not subject to the effects of the upstream vacuum. A further reason for leveling off the maximum porosity within the samples was that the bead would visibly steam during extrusion at these higher moisture levels. This indicates that at some point, the difference in pressure between the water vapor inside the material and the ambient atmospheric pressure would allow the moisture to rapidly escape the molten polymer before it could solidify and trap the remaining vapor. Under this condition, the sheer volume of vapor being formed overwhelmed any reductions in porosity from the vacuum.

2.7. Effect of vacuum hopper at different reinforcement levels

Previous observations in LFAM printing had indicated that porosity was relatively insignificant in unreinforced polymers but was a significant issue for reinforced materials [11,13,17]. It was thought that reinforcing fibers dramatically increase the interfacial surfaces available in a material on which a pore can nucleate, so without these nucleation sites, porosity was less likely to occur. Therefore, the pelletized feedstocks of neat ABS were mixed with either 20 %CF-ABS or 40 %GF-ABS to create a range of reinforcement content. Fig. 9 shows that for a conventional hopper system, the porosity of a CF-reinforced sample increases from < 1 % to ~5 % as the fiber content increases from 0 wt% to 10 wt%, and then holds constant (4 % - 5 %) as the fiber content continues to increase to 20 wt%. By contrast, the vacuum hopper approach was able to maintain porosity below 2 % (and often <1 %) across the full range of CF content. Fig. 10 shows similar trends for GF-reinforced

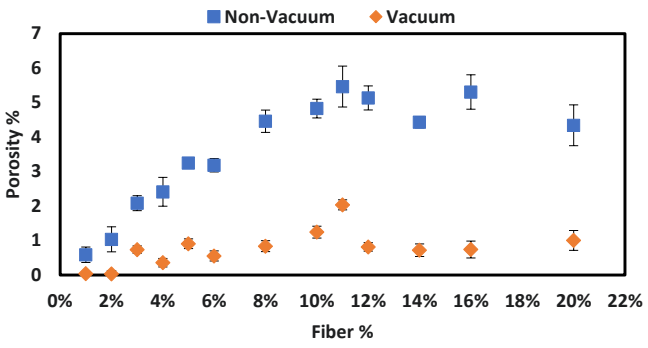

Fig. 9. The porosity of CF-ABS samples as a function of fiber reinforcement with either a conventional hopper or a vacuum hopper.

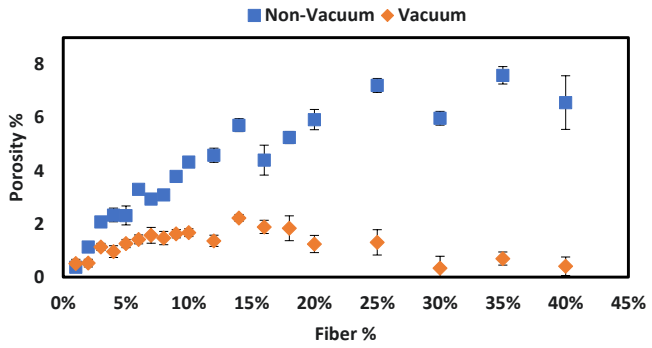

Fig. 10. The porosity of GF-ABS samples as a function of fiber reinforcement with either a conventional hopper or a vacuum hopper.

material, where the porosity increased to ~7 % before stabilizing with the conventional hopper but primarily maintained a porosity of 1 % - 2 % across the full range of fiber content with the vacuum hopper. The observed behavior in both cases of increasing porosity with fiber content until a stable level is maintained may be due to pore nucleation points increasing as additional interfaces are introduced but then eventually saturating. There is a slight increase in porosity for the vacuum hopper approach when extruding GF-ABS in the range of 5 wt% - 25 wt% before declining to lower levels at higher fiber content was a repeatable trend that is not well understood at this point. The authors hypothesize that since several of these tests were made with hand-mixed batches of pellets, the un-mixed samples at 0 %, 20 %, or 40 % show lower porosity because they were made with pellets taken directly from the oven while all others had to be weighed and mixed. This process would take a few minutes and necessitated the pellets be exposed to atmospheric moisture, which increased porosity as detailed in an earlier section.

2.8. Effect of vacuum hopper on larger platform extruder

The preceding experimental results were taken using a benchtop Randcastle extruder. In order to evaluate the effectiveness of the vacuum hopper approach to LFAM, a similar hopper was developed for a larger-scale extruder (Strangpresse) that is typically used on the BAAM or AM-CM systems. The primary approach used on the Randcastle extruder was repeated on the Strangpresse extruder with the exception that the vacuum applied to the Strangpresse system was limited to −10 to −15 in Hg (-266 to −380 Torr). The experimental setup for the benchtop study (Randcastle) was much simpler than the large-scale system (Strangpresse), with far fewer leaks and a different vacuum pump model. Therefore, similar vacuum levels were not able to be achieved on both systems. Even with a lower level vacuum applied to the hopper, Fig. 11

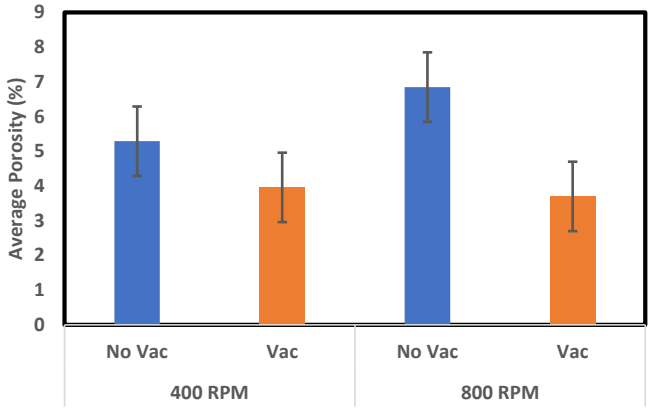

Fig. 11. The porosity of 20 %CF-ABS samples extruded with a Strangpresse system using a conventional hopper or a vacuum hopper.

shows that the vacuum hopper was still quite effective at reducing the porosity at two different extrusion speeds for 20 %CF-ABS. In particular, using the Archimedes method, it is observed that the vacuum hopper was able to reduce the porosity at the higher extrusion speed (800 RPM) by 45.9 %, from 6.9 % to 3.7 %, with a standard deviation of 0.45 and 0.79, respectively. This indicates that the vacuum hopper approach can effectively reduce porosity across multiple scale platforms and can be applied successfully to LFAM printing systems.

The XCT data analysis using ImageJ software to calculate the porosity in 800-RPM samples (with and without vacuum) is shown in Figs. 12 and 13. Fig. 12 illustrates a comparative analysis between two individual representative slices from the vacuum and non-vacuum processes, where white regions represent pores. It can be observed that the non-vacuum process exhibits larger pores within the slice than the vacuum process, although the number of pores is higher in the vacuum process. Fig. 13 shows a graph comparing the complete stacks of both processes. Porosity values obtained using XCT method are comparable to those obtained via Archimedes method and show a roughly 35 % reduction in porosity with a vacuum-assisted extrusion process.

2.9. Effect of vacuum hopper on smaller pores

The vacuum hopper approach was anticipated to affect the larger porosity observed in printed materials primarily. The larger pores were thought to have developed as tiny bubbles early in the extrusion process and then grew during the extrusion process via either Ostwald ripening or coalescence. Since the negative pressure of the vacuum hopper would have a more significant impact on the evolved gases earlier in the extrusion process, it was thought that the vacuum hopper would primarily affect larger pores and leave smaller pores relatively unaffected. Despite differences in porosity observed with tomography and the Archimedes method, SAXS data did not show any evidence of effects due to the vacuum treatment up to the length scales to which SAXS is sensitive (< 2 microns). Hence, it can be assumed that a lower limit to which the vacuum treatment is effective is 2 microns or larger. The SAXS data is shown in Fig. 14.

Further analysis of the SAXS data was not attempted since this theoretically could render a pore size distribution at this small scale but would not contribute to a deeper understanding of the effects of the vacuum treatment, which is the subject of this manuscript.

2.10. Theoretical explanation and pore distribution analysis

Pores are formed due to the mechanical entrapment of air or via the nucleation process. These pores may grow through the diffusion of water vapor or air, agglomeration with surrounding pores, or an increase in the temperature and the pressure. When the internal pressure inside the pore is equal or higher than the surrounding hydrostatic pressure (vacuum pressure), the pore may remain stable or grow [18]. This phenomenon describing pore stability or growth is due to water vapor or gas diffusion across the pore-polymer interface [19]. The pore stability for the spherical shape of pores can be expressed as follows,

$$\Delta P = P_{\text{int}} - P_{ext} = \frac{4\gamma}{D} \tag{1}$$

Where ΔP is pressure difference at the pore-polymer interface, P_{int} and P_{ext} are the internal pore pressure and external hydrostatic pressure on the polymer, respectively; γ is the surface tension at the polymer-pore interface, and D is the pore diameter. The difference in pressure in Eq. (1) is balanced by the surface tension acting on the polymer–pore interface. Furthermore, the pore pressure has two parts [19]:

$$P_{\text{int}} = P_{air} + P_w \tag{2}$$

where P_w and P_{air} are the pressure of water vapor and air, respectively. If the external or vacuum pressure P_{ext} is not sufficiently large enough to

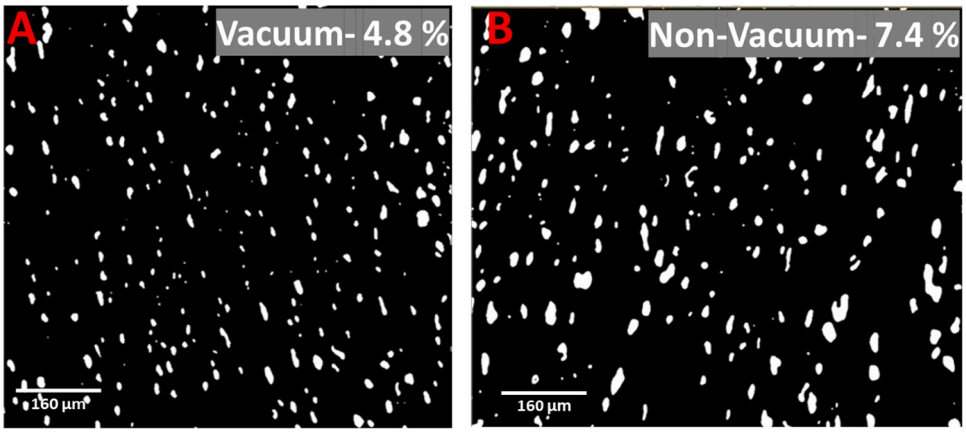

Fig. 12. Pore Visual for Vacuum and Non-Vacuum extrusion at 800 RPM on a LFAM system. The reduction of the pore size in the vacuum-treated samples is evident, but the increase in the total number of pores is also observed.

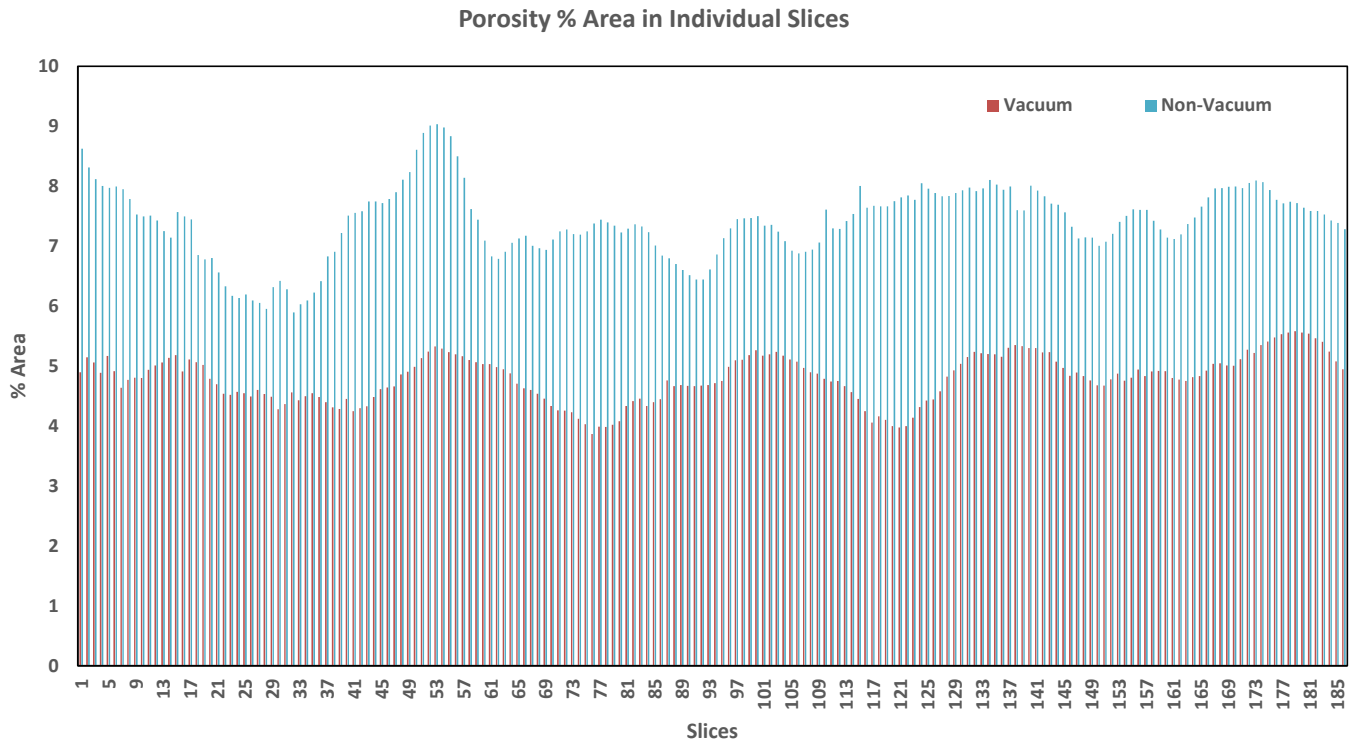

Fig. 13. Pore % area (cross-section of pores in 2D) in individual Slices for Vacuum and Non-Vacuum extrusion at 800 RPM on an LFAM system.

counterbalance P_{int}, the gas inside the pore will expand, causing the pore to grow (diameter D increases) and the internal pressure (P_{int}) decreases until equilibrium is reached. As per the Ideal Gas Law, the relationship between pressure (P), volume (V), the number of moles (n), and temperature (T) is given by the equation:

$$PV = nRT \tag{3}$$

where R is the universal gas constant. The product of P and V must remain constant if the number of n and T are unchanged. This behavior is further clarified by Boyle's Law, which states that for a fixed amount of gas at a constant temperature, the pressure of the gas is inversely proportional to its volume:

$$P \propto \frac{1}{V} \text{equivalently} P_1 V_1 = P_2 V_2 \tag{4}$$

where P_1 and V_1 are the initial pressure and volume, and P_2 and V_2 are the pressure and volume after a change, respectively.

Conversely, when more vacuum is applied, the P_{ext} around the pore increases. If P_{ext} exceeds P_{int}, net pressure (ΔP) at the pore-matrix interface becomes negative, which causes the pore to shrink, as illustrated in Fig. 15. This higher P_{ext} compresses the gas inside the pore, forcing it out, which reduces the pore's volume and decreases its diameter D until equilibrium is reached.

This behavior can be noticed from the XCT analysis (see Figs. 12 and 13) that the vacuum condition exhibits smaller pore than the non-vacuum condition. However, the total number of pores obtained from 186 slices are 47,518 and 64,562 for non-vacuum and vacuum conditions, respectively. The reason for higher number of smaller pores in vacuum condition could be due to possibilities of i) when pore shrinks, and the gas confined within the pores escapes which can nucleate smaller pores within matrix and ii) when the pores shrink beyond a certain point, they become unstable due to increased curvature (1/R)

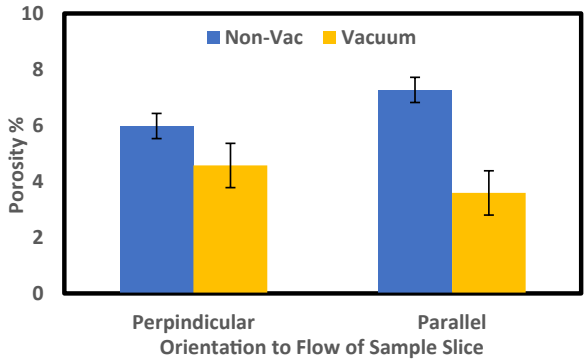

Fig. 14. The porosity of 20 %CF-ABS samples cut in orthogonal orientations extruded with a Strangpresse system, measured using the Archimedes method, to be further tested using SAXS.

and internal pressure inside the pore. At one point, the pressure becomes too high, the surface tension is no longer sufficient to keep the pore intact which can cause the pores to break up into further smaller pores. The behavior can be understood from Rayleigh-Plateau instability which describes how a cylindrical liquid column breaks up into smaller droplets to minimize surface area and achieve a more stable configuration. Although the number of pores is higher in vacuum process the resultant volume fraction is still smaller due to notable reduction in the pore size compared to non-vacuum condition.

Fig. 13 shows the % pore area obtained from XCT analysis for vacuum and non-vacuum extrusion at 800 RPM on an LFAM system. Fig. 16 shows the histogram of pore numbers with % pore area for non-vacuum and vacuum-assisted samples. The distribution of the pore area follows a Gaussian (normal) distribution, indicating a common spread around a central value. The % area range of pores is approximately 6–9 % for non-vacuum-assisted samples and 4–6 % for vacuum-assisted samples. The total number of pores counted is 47,518 for non-vacuum conditions and 64,562 for vacuum conditions. This indicates that vacuum assistance reduces the average % pore area by ~33 % while increasing the total number of pores by approximately 36 %.

Furthermore, the pores of % area range 7.25–8 % and 4.75–5.25 % are more in numbers for non-vacuum and vacuum conditions, respectively as evident from the higher peak values in Fig. 16. The shift in peak values demonstrates that vacuum conditions result in a finer distribution of smaller pores, while non-vacuum conditions tend to produce fewer but larger pores. Overall, vacuum conditions significantly influenced pore characteristics by increasing the total number of pores while reducing the average % pore area.

3. Demonstration of vacuum-extrusion on LFAM

The proposed vacuum-assisted extrusion process was further implemented in an actual Large Scale Additive Manufacturing process. The system employed was the Additive Manufacturing-Compression Molding (AM-CM) system, located at the Manufacturing Demonstration Facility, Oak Ridge National Laboratory. Only the AM portion (68 Kg/hr extruder on a 300-kg payload Kuka robot) of the AM-CM system was used to manufacture two 3D printed single bead rectangular boxes (190 mm×150 mm x 8.4 mm) with 20 % GF-ABS material using the following parameters as shown in Table 1.

One part was printed traditionally (without a vacuum), while the second part was printed while applying a −20 Hg vacuum in the material feeding section. The same prismatic hopper was used for both as shown in Fig. 17.

The porosity and surface quality of the printed parts were investigated. The inset in Fig. 17, shows the enlarged view of non-vacuum and vacuum-assisted printed boxes. The porosity was measured using an intensity-based image processing method, and found to be 9.10 % for non-vacuum samples and 2.29 % for vacuum-assisted samples (Fig. 18). The porosity was reduced by ~75 % when vacuum is applied in the

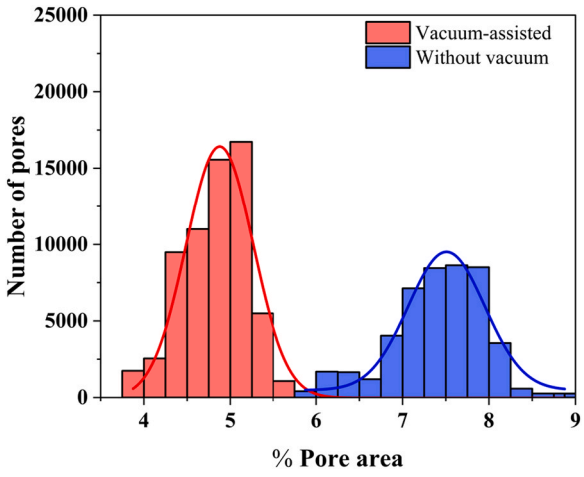

Fig. 16. Histograms for pore size distribution and Gaussian fitting for Vacuum and Non-Vacuum extrusion at 800 RPM on an LFAM system.

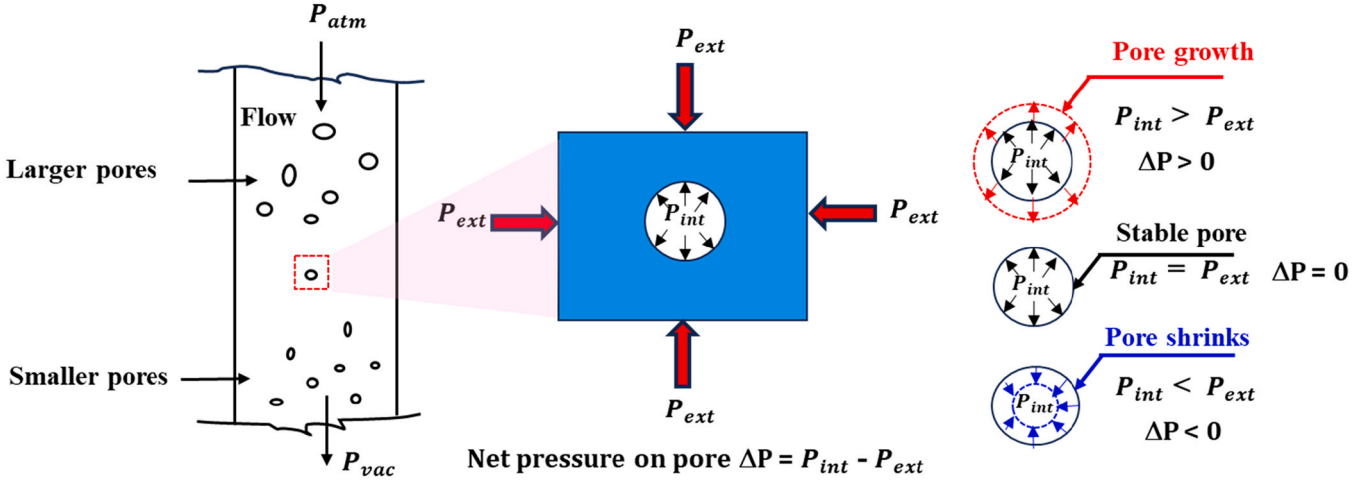

Fig. 15. Schematic diagram of polymer flow through a pipe to understand the pore size distribution. On the atmospheric pressure side, formation of larger pores is due to air entrapment during the flow. While the vacuum pressure side has smaller pores due to the removal of gas within pores by the vacuum.

Table 1
The process parameters considered for 3D printing rectangular boxes.

Nozzle diameter	7.62 mm
Extrusion speed (screw)	75 RPM
Extrusion Temperature	250 °C

material feeding system. However, the reduction in porosity was accompanied by a noticeable increase in surface roughness which could be due to altered material flow dynamics. Applying a vacuum in the material feeding section reduces the entrapped air and eventually gas in the polymer melt, significantly lowering porosity. However, if the applied vacuum pressure is high, it disrupts the pellet feeding into the extruder causing "starve-feeding" or "non-uniform" conditions. Starve feeding creates instabilities (varying pressure/shear forces) in the extrusion flow, that could create noticeable undulations, surface fracture, or "shark-skin" on the bead's surface [20,21]. In summary, an optimal vacuum pressure is paramount for high surface quality printing with reduced porosity.

To achieve low surface roughness alongside reduced porosity, future work could focus on optimizing extrusion parameters and material formulations (e.g. larger and heavier pellets). Strategies might include experimenting with controlled vacuum levels to strike a balance between porosity reduction and flow uniformity, fine-tuning extrusion speeds to minimize extrusion inconsistencies. Advanced nozzle designs that promote even deposition and post-processing techniques, such as surface tempering (smoothing), could also help mitigate the surface roughness.

3.1. Effect of vacuum condition on mechanical properties

Tensile testing was performed on standardized samples prepared from printed boxes to evaluate the mechanical properties along different directions: X (printing direction) and Z (across-layers). Specimens were machined to dimensions of ~114 mm in length, 6.0 mm in width, and 8.3 mm in thickness. The tensile tests were performed using an Instron universal testing machine with a load cell capacity of 20 kN. An extensometer with a gauge length of 50 mm was attached to the specimens to measure elongation. Tests were conducted at a crosshead speed of 2 mm/min. During testing, force and elongation data were continuously recorded until specimen failure. Ultimate tensile strength and tensile modulus were calculated from the recorded data in the X and Z direction, respectively.

Fig. 19 and Table 2 present the tensile strength and tensile modulus in the X and Z directions for both vacuum and non-vacuum-assisted samples. The results indicate that the tensile modulus is 0.94 % higher in the X direction and 5.39 % higher in the Z direction for vacuum-assisted samples compared to non-vacuum-assisted ones. The tensile strength improves by 12.62 % in the Z direction but was found to decrease by 6.14 % in the X direction with vacuum assistance. According to traditional fracture mechanics, the reduced porosity should have increased the strength of the polymer composite in the X-direction. However, these results indicated a decrease in tensile strength in the X-direction for vacuum-assisted samples. The authors believe that this behavior could be due to several other factors. One primary reason might be the fiber orientation. Due to altered material flow dynamics during the vacuum-assisted process, fibers might align in a manner that is less optimal for tensile strength in the X direction compared to non-

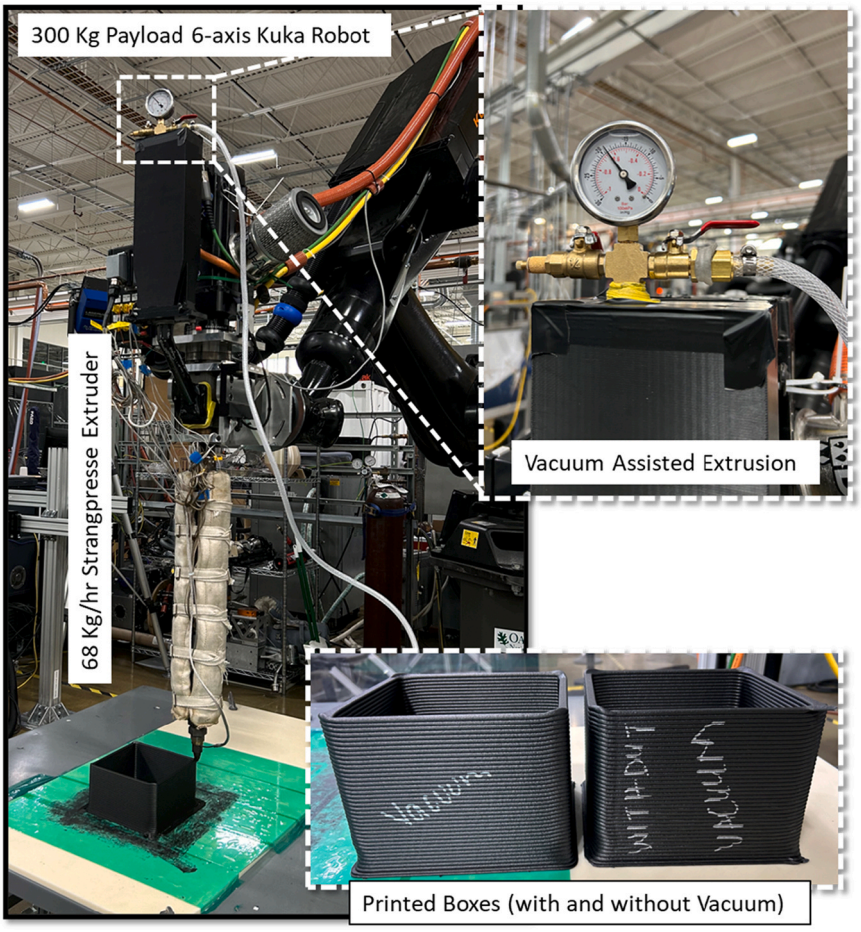

Fig. 17. Vacuum-assisted extrusion process in an actual Large Scale Additive Manufacturing process to reduce porosity in the printed parts.

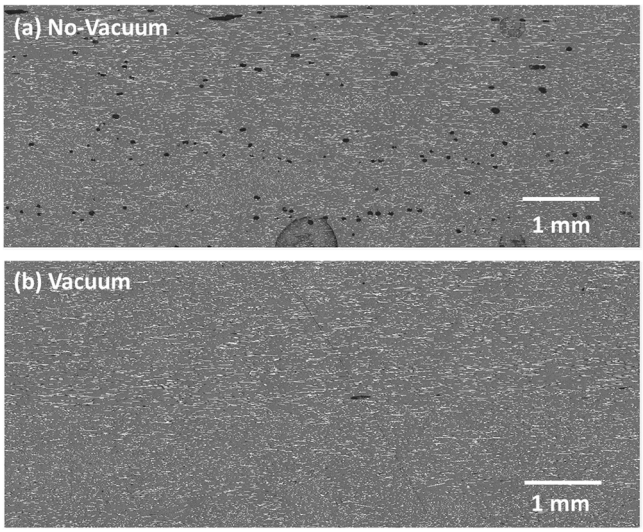

Fig. 18. Optical images (a) no-vacuum and (b) vacuum-assisted printed parts. The porosity was reduced by ~75 % when the vacuum is applied in the material feeding system.

vacuum conditions. Additionally, the increase in surface roughness due to the vacuum process, might have created surface irregularities that reduce structural integrity and increase susceptibility to failure under tensile loads.

The current work demonstrates the effectiveness of vacuum-assisted extrusion processes in reducing porosity in batches. However, an in-line vacuum hopper design, as detailed in the pending patent by Kumar et al. [22], is anticipated to provide a more consistent material feed while maintaining vacuum pressure (see Fig. 20). This system-level approach will be the focus of future investigations. The duration for which the pellets remain under vacuum can be adjusted by varying the hopper volume.

Since the pellets are pre-dried using an air-drying system before being fed into the vacuum hopper, the vacuum duration is not expected to significantly affect their moisture content or morphology. The primary challenge is likely to be maintaining a stable vacuum pressure throughout the printing process. As the in-line vacuum hopper involves the periodic opening and closing of valves in the hopper compartments, fluctuations in vacuum pressure could occur. This manuscript has also noted that different vacuum pressures result in varying levels of porosity reduction in the printed beads.

Overall, vacuum application was found to reduce porosity significantly when utilized on an actual AM system. However, additional investigation and adjustments are required to fine-tune the vacuum settings and balance the reduction in porosity with acceptable sample quality and mechanical properties.

4. Conclusions

A vacuum hopper approach has been proposed as a way to reduce porosity in fiber-reinforced materials relevant to LFAM printing. Experiments using a benchtop extrusion system from Randcastle have shown that the vacuum hopper approach can effectively reduce porosity in 20 %CF-ABS to less than 2 % across a wide range of deposition speeds (a 66 % reduction in porosity on average). The vacuum hopper also effectively reduced porosity associated with moisture uptake in samples exposed to ambient conditions for several hours following drying. The porosity of fiber-reinforced samples was shown to increase significantly with fiber content, increasing from < 1 % to ~4 % for CF-ABS and from < 1 % up to ~7 % for GF-ABS. In each case, the vacuum hopper could limit porosity to below 2 %, regardless of fiber content.

The vacuum hopper system worked on larger-scale platforms relevant to LFAM printing. 20 wt%CF-ABS samples produced at 800 RPM on a Strangpresse extruder showed a porosity of 7.4 % without the vacuum hopper system but only 4.8 % when the vacuum hopper was utilized. In an actual LFAM printed part, porosity was reduced by 75 % in vacuum-assisted process. X-ray tomography and Small-angle X-ray scattering allowed us to determine the effects of the vacuum treatment on porosity that occurs on a length scale > 2 microns. Currently, the vacuum hopper approach is restricted to batch processing, but a patent-pending approach for implementing this technique on a continuous deposition printer has been developed and will be the subject of future research.

Author Statement

Thank you for the opportunity to revise the manuscript entitled "Vacuum-Assisted Extrusion to Reduce

Internal Porosity in Large-Format Additive Manufacturing." As detailed within the Response to

Reviewers, we have made the requested minor revisions to the

Table 2
Mechanical properties of 3D printed parts with or without vacuum assistance.

	X-direction		Z-direction	
	Tensile strength (MPa)	Tensile Modulus (MPa)	Tensile strength (MPa)	Tensile Modulus (MPa)
Non-Vacuum	73.75 ± 5.37	12.70 ± 0.32	15.60 ± 1.49	2.41 ± 0.04
Vacuum-assisted	69.22 ± 4.50	12.82 ± 0.64	17.57 ± 0.77	2.54 ± 0.13
	Decrease of 6.14 %	Increase of 1.0 %	Increase of 12.62 %	Increase of 5.39 %

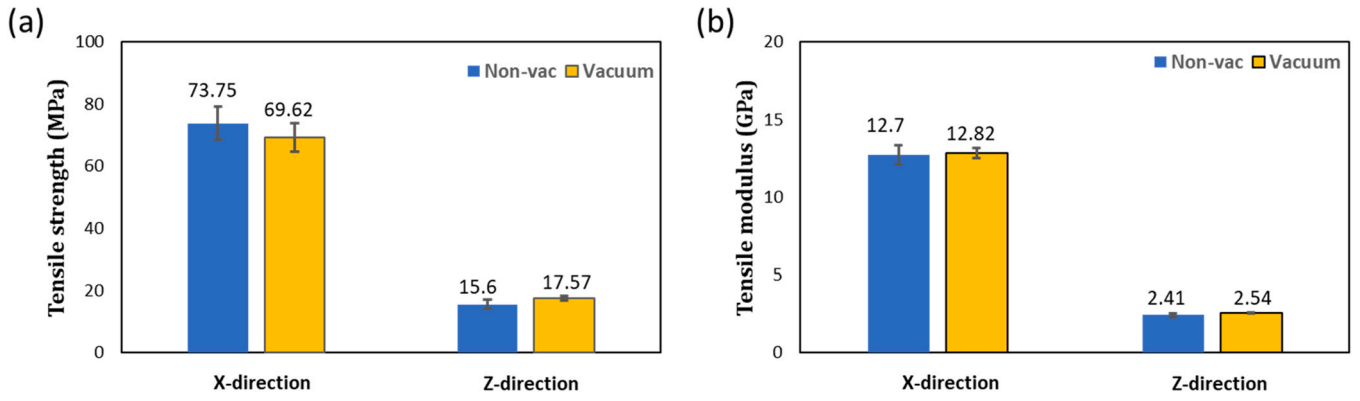

Fig. 19. Mechanical properties of 3D printed parts with or without vacuum assistance.

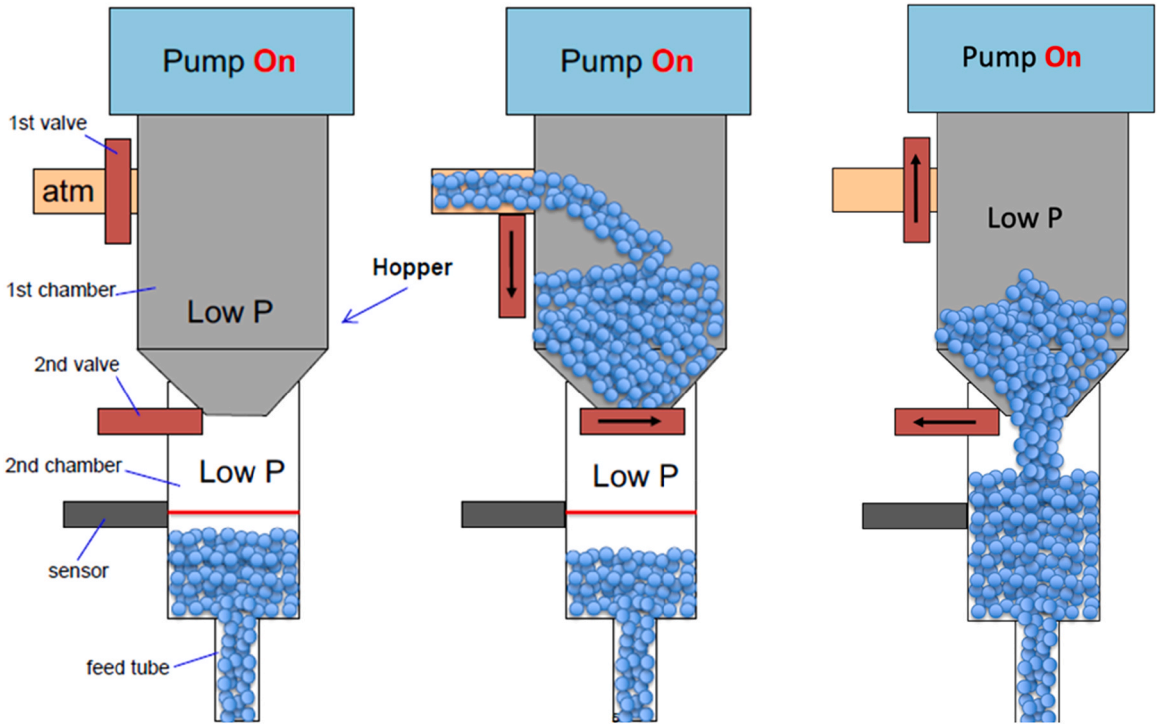

Fig. 20. Novel vacuum hopper design for continuous printing [22].

manuscript.

CRediT authorship contribution statement

Vlastimil Kunc: Writing – review & editing, Funding acquisition, Conceptualization. **Chad Duty:** Writing – review & editing, Writing – original draft, Supervision, Project administration, Methodology, Funding acquisition, Conceptualization. **Frye Mattingly:** Writing – review & editing, Writing – original draft, Methodology, Investigation, Formal analysis, Data curation, Conceptualization. **Vipin Kumar:** Writing – review & editing, Methodology, Investigation, Conceptualization. **Komal Chawla:** Writing – review & editing, Validation, Investigation, Data curation. **Wim Bras:** Writing – review & editing, Investigation, Formal analysis, Conceptualization.

Declaration of Competing Interest

The authors declare the following financial interests/personal relationships which may be considered as potential competing interests: Several co-authors have a patent pending regarding this technology (Patent Application 18/771,173). One of the authors, Chad Duty, has previously served as an Associate Editor for this journal. Authors declare that they have no other known competing financial interests or personal relationships that could have appeared to influence the work reported in this paper.

Acknowledgements

The authors gratefully acknowledge support from the Composite Core Program (CCP 2.0), supported by Vehicle Technology Office, Office of Energy Efficiency and Renewable Energy, U.S. Department of Energy. A portion of the research was also sponsored by the U.S. Department of Energy, Office of Energy Efficiency and Renewable Energy, Advanced Manufacturing Office, under contract DE-AC05–00OR22725 with UT-Battelle, LLC. This material was also based upon work supported by the National Science Foundation under Grant No. 2055529. Feedstock materials used in this work were provided by TechmerPM, TN, USA. The authors acknowledge the assistance of Dilworth Parkinson of the Advanced Light Source, which is a DOE Office of Science User Facility under contract no. DE-AC02–05CH11231. Authors also thank Dr. Segun Isaac Talabi and Brittany Rodriguez for assisting in vacuum-assisted LFAM prints.

Data availability

Data will be made available on request.

References

[1] C.M.S. Vicente, et al., Large-format additive manufacturing of polymer extrusion-based deposition systems: review and applications, Prog. Addit. Manuf. 8 (6) (2023) 1257–1280.
[2] A. Roschli, et al., Designing for Big Area Additive Manufacturing, Addit. Manuf. 25 (2019) 275–285.
[3] V. Kumar, et al., High-performance molded composites using additively manufactured preforms with controlled fiber and pore morphology, Addit. Manuf. 37 (2021) 101733.
[4] Kumar, V., et al., *Large-scale continuous carbon/glass fiber additive-compression molded composites*, in *Conference: CAMX: The Composites and Advanced Materials Expo. Dallas, Texas, United States of America*. 2021. ⟨https://www.osti.gov/biblio/1831656⟩ (accessed December 13, 2024).
[5] Lorenzana, R. and F. Adrian, *Thermal Characterization of ABS/Carbon Fiber, ABS/Glass Fiber and PETG/Glass Fiber Reinforced Composites Used in Large Area Additive Manufacturing*. 2019, (Dissertation) University of Texas, El Paso.⟨https://scholarworks.utep.edu/dissertations/AAI27669549⟩ (accessed December 13, 2024).
[6] L. Love, et al., The importance of carbon fiber to polymer additive manufacturing, J. Mater. Res. 29 (2014) 1893–1898.
[7] H.L. Tekinalp, et al., Highly oriented carbon fiber–polymer composites via additive manufacturing, Compos. Sci. Technol. 105 (2014) 144–150.
[8] C. Duty, et al., Z-Pinning approach for 3D printing mechanically isotropic materials, Addit. Manuf. 27 (2019) 175–184.
[9] L. Malagutti, et al., Effects of printed bead volume on thermal history, polymer degree of crystallinity and mechanical properties in large scale additive manufacturing, J. Mater. Process. Technol. 316 (2023) 117961.
[10] D.M. Sánchez, et al., Development of carbon fiber acrylonitrile styrene acrylate composite for large format additive manufacturing, Mater. Des. 191 (2020) 108577.
[11] F. Caltanissetta, et al., In-situ monitoring of Material Extrusion processes via thermal videoimaging with application to Big Area Additive Manufacturing (BAAM), Addit. Manuf. 58 (2022) 102995.

[12] O. Eyercioglu, M. Aladag, S. Sever, Temperature Evaluation and Bounding Quality of Large Scale Additive Manufacturing Thin Wall Parts, Sigma J. Eng. Nat. Sci. 36 (3) (2018) 645–654.
[13] Hoskins, D., et al., *Development of Large Scale Extrusion Deposition for Structural Applications*. 2022. ⟨https://iacmi.org/wp-content/uploads/2022/01/IACMI-3.12-Final-Report-12.27.21-AMO-approved.pdf⟩ (accessed December 13, 2024).
[14] Mattingly, F.L., et al. *Characterizing internal porosity of 3D-printed fiber reinforced materials*. in *32nd Annual International Solid Freeform Fabrication Symposium – An Additive Manufacturing Conference*. 2021. University of Texas - Austin, USA. ⟨https://repositories.lib.utexas.edu/server/api/core/bitstreams/f6ed67dc-8a25-4159-808b-e8d18911d55f/content⟩ (accessed December 13, 2024).
[15] Z.A. Mohd Ishak, J.P. Berry, Effect of moisture absorption on the dynamic mechanical properties of short carbon fiber reinforced nylon 6, 6, Polym. Compos. 15 (3) (1994) 223–230.
[16] A. Tukachinsky, Y. Talmon, Z. Tadmor, Foam-enhanced devolatilization of polystyrene melt in a vented extruder, Aiche J. 40 (1994) 670–675.
[17] MacDowell, A., et al., *X-ray micro-tomography at the Advanced Light Source*. Developments in X-Ray Tomography VIII. 2012. 8506: p.850618 https://doi.org/10.1117/12.930243.
[18] J.L. Kardos, M.P. Duduković, R. Dave, Void growth and resin transport during processing of thermosetting — Matrix composites. Epoxy Resins and Composites IV, Springer Berlin Heidelberg, Berlin, Heidelberg, 1986, pp. 101–123.
[19] Y. Ledru, et al., Coupled visco-mechanical and diffusion void growth modelling during composite curing, Compos. Sci. Technol. 70 (15) (2010) 2139–2145.
[20] Kishore, V., et al., *Predicting sharkskin instability in extrusion additive manufacturing of reinforced thermoplastics*, in *28th Annual International Solid Freeform Fabrication Symposium – An Additive Manufacturing Conference*. 2017: Austin, Texas. p. 1696-1704.
[21] J. Molenaar, R.J. Koopmans, C.F.J. den Doelder, Onset of the sharkskin phenomenon in polymer extrusion, Phys. Rev. E 58 (4) (1998) 4683–4691.
[22] Kumar, V., et al., *Reducing Porosity of 3D Printed Composites using Pellet-fed Single-Screw Extrusion Systems| ORNL, (n.d.)*.⟨https://www.ornl.gov/technology/202305307⟩ (accessed December 13, 2024).